Study of the interaction between coherent structures and boundary layer in a Forced Turbulent Plane Jet Impinging on a Semi-Cylinder

Nabil KHAROUA[1*], Lyes KHEZZAR[1], Zoubir NEMOUCHI[2], Mohamed ALSHEHHI[1]

[1]Mechanical Engineering Department, Petroleum Institute, Abu Dhabi, United Arab Emirates
[2]LEAP, Département de Génie Mécanique, University Constantine 1, Constantine, Algeria
[*]Corresponding author: nkharoua@pi.ac.ae

Résumé

Un jet turbulent forcé, impactant sur un demi-cylindre, a été simulé en utilisant le modèle de simulation des grands tourbillons LES. Le jet est placé à une distance égale à deux fois la largeur de la buse. Le nombre de Reynolds, basée sur la largeur de la buse et la vitesse moyenne, est égal à 5600. Le jet est forcé à une fréquence de 600Hz.

L'étude se concentre sur les effets des structures turbulentes organisées, générées au niveau de la couche de cisaillement libre, sur la couche limite qui se développe le long de la surface courbée et le transfert thermique correspondant. L'interaction complexe est illustrée à travers le nombre de Nusselt et le coefficient de frottement exprime en terme de fréquences.

Le passage des tourbillons principaux, générés au niveau de la couche de cisaillement libre, induit des tourbillons secondaires dans la couche limite et entraîne à la fois l'air chaud du jet, et l'air froid de son entourage qui n'est pas souhaitable dans les applications de chauffage.

Mots-Clés: Impinging jet, Steady jet, Forced jet, Forcing frequency, Large Eddy Simulation

1. Introduction

Turbulent impinging jets are used in several industrial areas to achieve high efficiency heating/cooling/drying. They are also used in the process of controlling film thickness on coated metal products for which the distribution of shear stress and pressure is crucial.

Steady round and plane turbulent impinging jets were studied extensively in the literature [1]. Past studies, which mainly dealt with round jets impinging on plane surfaces, have identified three main regions characterized by a free jet, stagnation and wall jet. In addition, previous studies illustrated the important and intricate role that vortices, generated in the free jet shear layer, have on heat and momentum transfer on the target surface. When forced, turbulent jets exhibits a more coherent behavior allowing the identification of vortices more easily. The primary vortices, generated in the free jet shear layer, induce secondary vortices, on the target solid surface, by roll up of the boundary layer into an opposite signed vortex with sometimes a tertiary vortex. The secondary vortices are generated downstream of regions with boundary layer growth and can be separated undergoing a strong ejection from the wall layer [2]. Few experimental studies focused on the effects of coherent vortices, in circular jet configurations, on the boundary layer developing on flat impingement walls [3-5]. Naguib and Koochesfahani [3] investigated the effects of the vortices on the surface-pressure distribution by using measured velocity data and solving a Poisson's equation for pressure for a forced round jet. Secondary and tertiary vortices were seen to be generated due to the interaction of the primary vortices with the wall. The passage of the primary vortices close to the wall was associated with noticeable pressure signatures. El Hassan et al. [4] studied the effects of the coherent structures on the wall-shear stress distribution along the impingement wall. They noticed that the front part of the transverse vortex caused flow expansion resulting in an ejection of the fluid from the impinging wall and, consequently, reducing the wall shear stress. Hubble et al. [5] devoted their experiments to the effects of the vortical structures on

the heat transfer for cooling applications. They stated that the passage of a coherent structure close to the impingement wall generates three distinguished flows. The maximum heat transfer occurs upstream of the vortex due to a downwash stream causing the entrainment of cold air from the outer region. A stream parallel to the wall, underneath the vortex, decreases the heat transfer because the air has already gained some heat. An upwash stream, downstream of the vortex, decreases the heat transfer to its minimum.

When impinging jets are forced, their behavior and their natural frequency may differ from that of a free jet for small nozzle-to-wall distances [6]. In terms of numerical simulation, previous studies used mainly the Reynolds-Averaged Navier-Stokes (RANS) approach. Very few contributions have tackled the complex problem of forced jets. Among these, Tsubokura et al. [7] used DNS and LES to study round and plane impinging jets on a plane surface. They forced both jets with a Strouhal number (St), based on the inlet velocity and dimensions, equal to 0.4 for both configurations. They mentioned that no clear dominant frequency was observed for the steady plane jet. Hofmann et al. [8] compared 13 RANS-based turbulence models in the computation of heat transfer of unforced and forced jets. The SST k-w model was found to perform best in predicting the Nu distribution. Uddin et al. [9] used the LES turbulence model to simulate a forced round jet impinging on a flat plate. They found that forcing the jet at the preferred mode of a round jet and its sub-harmonics generated large vortical structures that strike the flat target surface. On the other hand, forcing the jet at harmonics suppresses the structures and alters the jet efficiency in enhancing heat transfer. They also observed an attenuation of the well-known second peak of the Nusselt number under the effects of forcing. As a conclusion from the literature, studies on forced impinging jets with a focus on the interaction between the vortex structures and the surface boundary layer are scarce. It is also evident that most studies focused on round jets impinging on a plane surface.

The present work investigates the detailed behavior of a forced plane turbulent jet impinging on a curved surface placed at a distance of two nozzle widths. Contrary to previous studies, this contribution addresses the effects of coherent vortices and their interaction on more than one parameter. The study is devoted to the behavior of the shear stress and heat transfer rate on the wall simultaneously. LES is used to resolve the details of large eddy structures and hence investigate thermofluid dynamics on a spatial and temporal scale. The plane jet was forced at a frequency equal to 600Hz and amplitude equal to 30% of the mean jet velocity.

2. Numerical approach

2.1. Mathematical and numerical modeling assumptions

The flow is assumed incompressible, unsteady and turbulent. The commercial software ANSYS FLUENT 14.0 [10] was used to solve the filtered continuity, momentum and energy equations. Details of the mathematical model used can be found in the documentation of ANSYS FLUENT 14.0 [10]. Thus, it is briefly presented herein without details of the set of equations solved. The subgrid stress accounting for the unresolved scales contribution is modelled using the Boussinesq hypothesis. The Smagorinsky constant is dynamically calculated based on the information included in the resolved scales of motion [11-12].

2.2.Mesh quality

The geometrical configuration (Fig. 1) and experimental results used in this study are extracted from Chan et al. [13]. A low turbulence heated rectangular plane air jet was blown downstream of a contracting slot nozzle with a width W=6.25mm impinging on a semi-cylindrical convex surface of diameter D=150mm. The distances from the slot exit to the point of impact on the curved wall considered in this study is H=2W. The Reynolds number, based on the slot width and the uniform

jet velocity at the slot exit, is Re_W=5,600. The classical grid independency tests yield a DNS simulation when applied to LES [14-17]. Usually, the efficiency of a computational grid for LES simulations is assessed through some parameters such as the turbulence length and time scales, the percentage of resolved turbulent kinetic energy, and a priori and posteriori validation [17]. In the present study, the computational domain was divided into 16.5 million hexahedral computational cells. The grid was refined in the three characteristic regions of the flow, namely, the free jet, the impingement region, and the wall jet. The recommended cell size, used explicitly as a filter width, should be around 12 times the Kolmogorov scale [18]. In the present work, the ratio was less than 15.75 based on a Kolmogorov scale of approximately 20 microns estimated from a RANS simulation of the same case using the Reynolds stress turbulence model. In addition, grid sizes can be compared to estimates of the Taylor scale or 1/10 of the integral scale [19]. The estimates of these scales were found equal to 0.1 mm and 0.6 mm respectively, which confirms that the present mesh is reasonably fine. The non-dimensional distance from the curved wall (y+) was smaller than 1 in the region of interest (s/W=0-10) with a maximum equal to 2 outside this region. It is worth to mention that two other coarser meshes of 4.6 and 6.5 million cells were used previously to simulate the same case [20, 21].

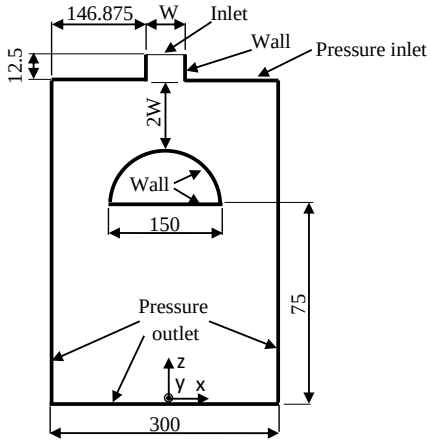

Figure 1: Problem configuration (not to scale) and types of boundary conditions

2.3.Boundary conditions

Figure 1 illustrates the types of boundary conditions used. The fluid enters the domain with a uniform velocity through a channel whose width is W and length 2W. The exiting plane jet is characterized by a uniform velocity within its core and a thin boundary layer on either side [13]. The inlet boundary conditions, taken from the experimental results of Chan et al. [13], are an imposed mean velocity of 14.87 m/s and a turbulence intensity of 2 %. Fluctuating velocities were generated using the spectral synthesizer technique [10]. The velocity at the inlet u_{in} was prescribed using Equ. 1 to force the steady jet at a frequency f equal to 600Hz.

$$u_{in} = 14.87\left[1 + 0.3\sin\left(2\pi ft\right)\right] \quad (1)$$

The forcing frequency *f* was chosen to yield a Strouhal number above the critical value of 0.2 mentioned by Hoffmann et al. [22] and to correspond to the range of dominant Strouhal numbers for plane jets. The Strouhal number, based on the initial boundary layer momentum thickness of the jet just at its exit, was equal to 0.012 and 0.25 when based on the jet width which is consistent with the range of dominant Strouhal numbers for plane jets [23-24].

A zero-relative-pressure and a turbulence intensity of 0.1 % were prescribed on the top surfaces, on either side of the nozzle channel. On the bottom, left and right boundaries of the

domain, zero-relative-pressure boundary conditions were imposed with a turbulence intensity of 0.1 % in the case of fluid backflow into the domain.

In order to minimize the number of computational cells in the domain, periodic boundary conditions were applied on the two opposite faces, in the y direction (front and rear). The distance between the periodic boundaries was equal to 31.25 mm which is larger than twice the integral length scale [25].

A constant temperature of 291 K was prescribed on the semi-cylindrical wall and in the free-entrainment constant-pressure boundary regions where re-entry flow took place. The inlet jet had a constant temperature of 313 K.

2.4.Numerical tools and simulation strategy.

A bounded central differencing scheme was used to discretize the convective terms in the filtered Navier-Stokes and energy equations [10]. A steady mean flow was, first, computed using the k-ε model to provide reasonable initial conditions for the LES simulation. Subsequently, an LES simulation was conducted during more than 0.07 s corresponding roughly to the residence time of the flow based on an average velocity of 6 m/s and the domain height.

The integration time step used was 10^{-5} s. According to ANSYS FLUENT 14.0 documentation [10], the time step should be less than or equal to 1/20 the period of the vortex shedding which corresponds in our case to a maximum Strouhal number of 0.52 and which is adequate enough for the unforced jet. For the forced jet the time step represents 1/160 the period of vortex shedding. In addition, the Courant number based on the time step chosen and the mesh resolution was kept less than 2 [26]. When the flow stabilized, the statistics were collected over a time interval corresponding to more than six times the characteristic residence time.

The local time-averaged Nusselt number $\overline{Nu}(s)$ is calculated from N samples using

$$\overline{Nu}(s) = \frac{1}{N}\sum_{i=1}^{N} Nu(s, t_i) \qquad (2)$$

The simulations were conducted on a Linux HPCC machine. Each case was run using ANSYS FLUENT 14.0 parallel version on 48 processors during 360 and 550 hours of CPU time for the unforced and forced jets respectively.

3. Results and discussion

The time-averaged flow field is, first, presented to show the overall picture of the flow and to validate the numerical simulation results. The LES results were compared with the experiments of Chan et al. [13] in addition to studies from the literature for similar flows. Then, the instantaneous flow filed is illustrated to elucidate the sequence of phenomena occurring at different times during a chosen observation window and different positions along the curved wall.

3.1.Time-averaged field

The wall-shear stress is an important parameter related to impinging jets usage and operation (e.g., jet stripping). Figure 2 shows the distribution of the mean wall shear stress along the impingement wall. Experimental profiles of Tu et al. [27] and Tu and Wood [28] and theoretical profiles of Phares et al. [29], for a jet impinging on a flat plate, are presented for reference. The theoretical approach adopted by Phares et al. [29] is limited to the laminar region corresponding approximately to twice the jet width from the impingement point x/H<1 (H is the distance from the jet exit to the impingement point). The experimental and theoretical profiles exhibit a similar behavior with an increase towards a maximum value at the same location. The linear growth and

sharp decrease of the mean wall-shear stress occur within the laminar boundary layer region [29]. The second peak of the wall-shear stress, at x/H=3, was explained by the transition from the laminar to the turbulent regime. A good agreement, between the numerical results and those from the literature, is seen within the linear laminar flow region. However, the wall-shear stress first peak is higher than that for flat plates and its location is slightly shifted away from the impingement point. Similar observations are valid for the second peak which is normally followed by the development of the wall jet, except that the unforced jet peak is more pronounced than the forced jet one which displays lower shear stress in the wall jet region than the unforced jet. Animations of vorticity contours indicated that the location of boundary layer separation induced by the primary vortices occurs in the region x/H=1 and 2.

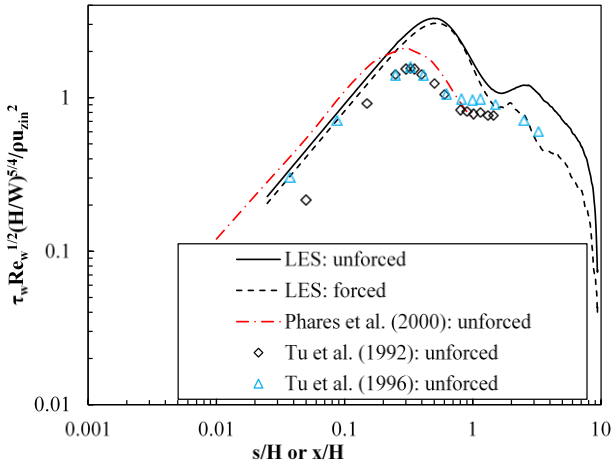

Figure 2: Mean wall shear stress distribution along the impingement wall from the stagnation point

The local time-averaged Nusselt number is illustrated in Fig. 3. A first peak is seen nearby the impingement region where the boundary layer is very thin. Then, it decreases away due to the thickening of the boundary layer. The Nusselt number reaches a dip at about s/W=2.6 for the unforced jet and second peak at about s/W=4.8 which is similar to that in the wall-shear stress distribution (Fig. 2). Similarly to the wall-shear stress distribution, the forced jet exhibits a second peak at about s/W=3.7. These results relatively agree with the experiments of Chan et al. [13]. However, the dip is quantitatively underestimated by the simulation. Forcing the jet caused a decrease of Nu at the impingement. A similar behavior was observed by Mladin and Zumbrunnen [6] for low jet-to-plate distances when the potential core impinges on the surface at stagnation. They attributed this to a thickening of the boundary layer due to the pulsations which reduce the heat transfer rate. Azevedo et al. [30] concluded that degradation in heat transfer for a pulsing jet is believed to be due to relatively low-magnitude small scale turbulent fluctuations superimposed on the instantaneous periodic flow. Heat transfer is a strongly dependent function of temporal flow structure. Turbulence intensity decreases with increasing pulse frequency.

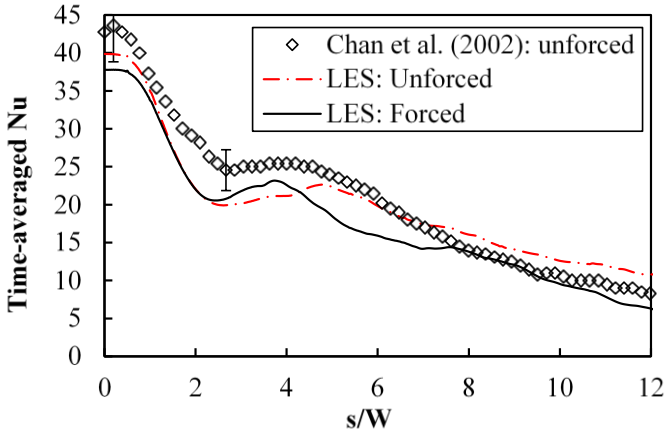

Figure 3: Mean Nusselt number along the impingement wall from the stagnation point

3.2.Instantaneous field

It is important to describe the trajectories of the vortices before discussing their interaction with the impingement wall. Figure 4 depicts the trajectories of the vortices from their point of generation to their disintegration. The primary vortices V1 and V2 are generated regularly and sequentially within the free shear layer of the emerging jet at the frequency of 600 Hz. They travel downstream following different trajectories to interact with the boundary layer forming on the curved target surface. This interaction generates secondary vortices V3 and V4 of opposite vorticity which will merge later to create V5. This sequence of phenomena is repeated systematically (Fig. 5) with slight differences for certain cycles. The observations are conducted by considering a temporal window that contains cyclic repeatable events involving the passage of V1 and V2 in the vicinity of the curved wall and their interaction with it

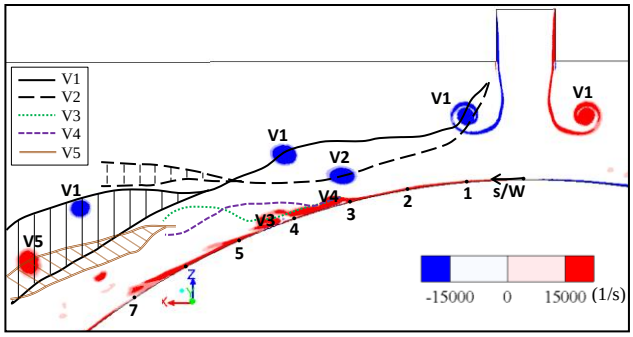

Figure 4: Trajectories of vortices (y vorticity component)

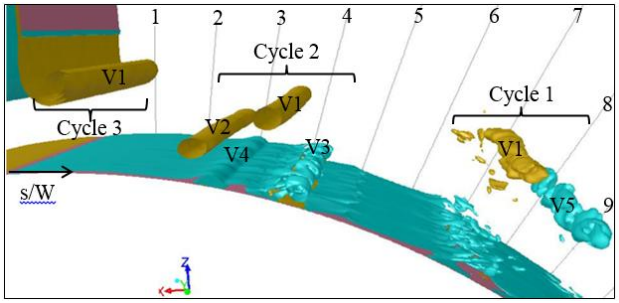

Figure 5: Groups of vortices representing periodic cycles

The starting time of the window is chosen arbitrarily to coincide with the passage of the primary vortex V1 above the point s/W=1 on the curved wall whereas the end time coincides with the passage of V1 above the point s/W=7 after approximately 5 ms from the starting time. The

behavior of the vortices can be better understood through their characteristic frequencies as shown in Figs. 6 and 7. These frequencies were extracted from velocity, Nusselt number and friction coefficient and correspond simply to the peaks of these parameters. A priori, it would be thought that peaks of Nu and Cf should correspond to vortex passage. However, it will be shown that this is not always the case.

Figure 6 shows that the dominant frequency at the jet exit (point a) corresponds exactly to the forcing frequency. This is expected since no particular phenomena occur at that location. Moving farther (point b), peaks at a frequency equal to 600 Hz and its harmonics reflect the successive passage of the two vortices V1 and V2 being generated at the forcing frequency. By observing animations, it was noticed that the harmonics correspond to the passage of V2 with an acceleration under the effect of V1's wake. At point c, the dominant frequency becomes 300Hz with harmonics until 1200Hz. The reason is that only V1 passes by point c while V2 passes slightly below. Thus, the dominant frequency of 300Hz corresponds to the passage of V1 which is characterized by a longer period between every two subsequent passages. At this point V1 and V2 follow different trajectories as shown in Fig. 4 which adds a degree of complexity to the interaction of the coherent primary vortices V1 and V2 with the boundary layer along the impingement wall.

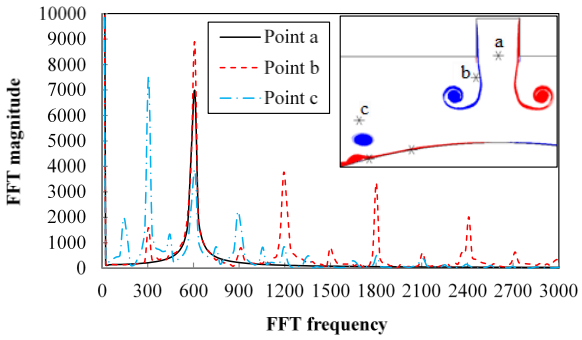

Figure 6: FFT of velocity signals at three points far from the wall

Fig. 7 presents FFT profiles extracted from time signals of Nu and C_f at different normalized distances, from the impingement point, along the curved wall. The distances are normalized by the jet-exit width. These profiles are meant to assess the correlation degree between the dynamic filed and heat transfer under the effect of the coherent vortices. Snapshots of the flow and temperature fields are shown in conjunction with the FFT profiles to explain the characteristic frequencies as a result of interaction between the coherent primary vortices and the boundary layer along the impingement wall. The right snapshot represents contours of vorticity while the left one represents contours of temperature. At s/W=2, Nu and Cf are perfectly correlated with a dominant peak at 300Hz since vortices V1 and V2 interact with the wall separately. Similarly to Fig. 6, the harmonics of 300Hz correspond to the acceleration of V2 under the effect of V1's wake. At s/W=3, Nu and Cf are de-correlated at 900Hz where a high peak of Cf FFT while Nu does not exhibit any noticeable peak. The corresponding snapshots show that although vortex V4 is acting at the location of probe 3, the cold air entrained by vortex V2 towards the wall causes Nu to decrease. This situation illustrates that the presence of recirculation zone does not imply a systematic increase of heat transfer. At s/W=4 vortices peaks of Nu are seen at 600Hz and 900Hz while a lower peak of Cf is senn at 600Hz and no peak of Cf at 900Hz. Referring to the snapshots, it can be seen vortex V3 has separated at probe 4 which explains the lower peaks of Cf whereas its entrainment effect is still strong. Also, V3 accelerates to reach V4 at s/W=4 which explains the combined effect (300Hz) rather than an individual effect (600Hz). Similar effects are observed at s/W=5 and s/W=6 where the separated vortices move farther away from the wall

while their entrainment effect persists. At s/W=6, a very high peak is seen at 600Hz due to the effect of vortex V5 which has resulted from the merging of V3 and V4.

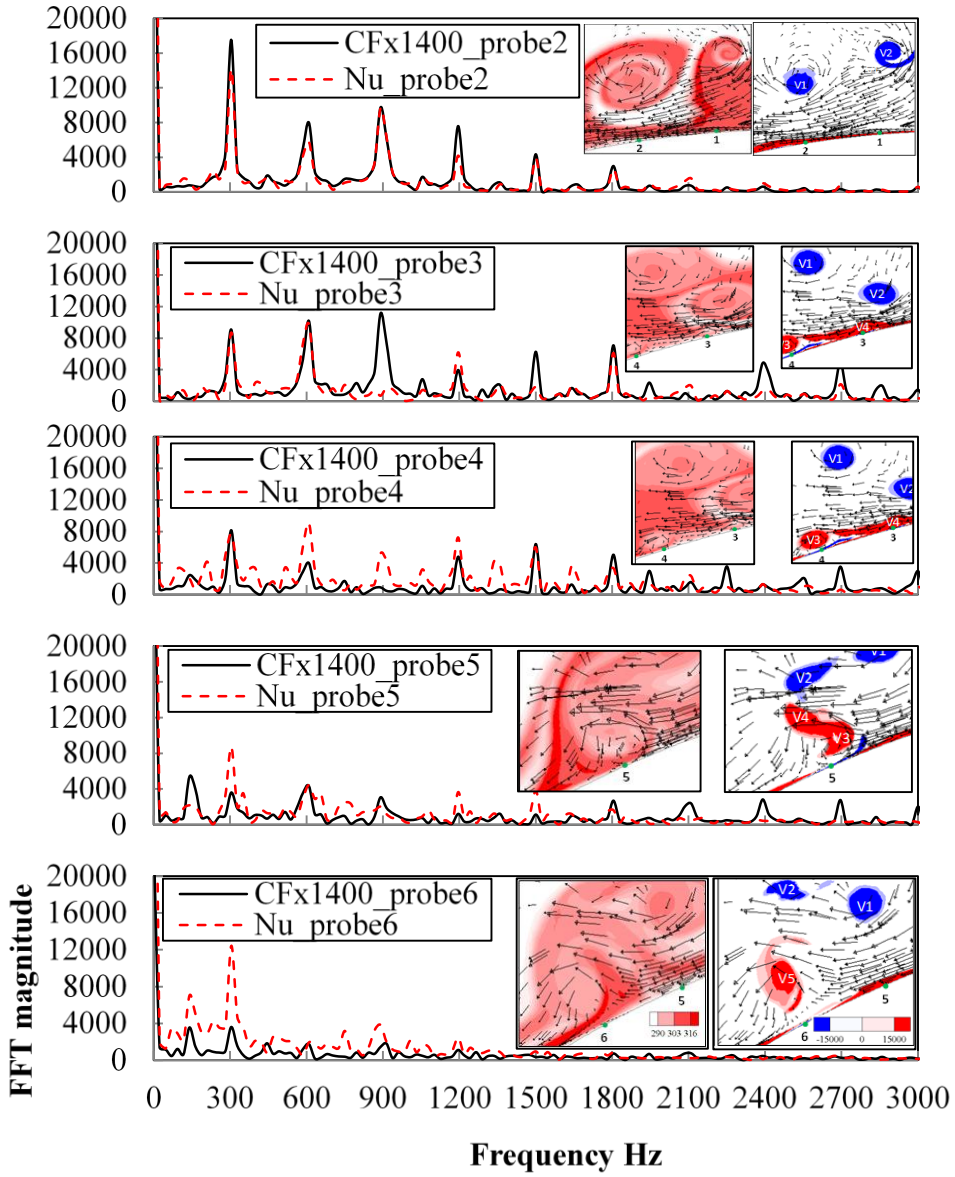

Figure 7: Profiles of FFT extracted from time signals of Nu and Cf at different locations on the wall

4. Conclusions

Large eddy simulation of forced impinging plane jet was conducted. The jet impinges on a convex semi-cylinder. The results of the unforced jet were validated using data extracted from different contributions in the literature. The forcing of the jet allows to generate an organized generation of vortices which maintain their coherence far downstream along the curved wall compared to the unforced jet.

Primary vortices are generated within the free shear layer close to the jet exit and could be grouped into quasi-periodical cycles. These primary vortices follow a different trajectory starting from a distance equal to about s/W=1. At this stage, different dominant frequencies manifest and cause a complex interaction between the primary vortices and the boundary layer along the curved wall.

This study extended previous contributions, focusing on one vortex at a time, to a combination of vortices in more complex flow structure. The flow conditions of the present study allowed to elucidate the effects of several complex phenomena such as the overtaking of one primary vortex by another, the effects of induced secondary vortices and their pairing when lifting from the surface.

The temperature field was found to be crucial for a better understanding of the interaction between the primary vortices and the boundary layer. Indeed, the vortices can entrain both hot and cold air from the jet and the surroundings respectively. It is clear that the purpose of the jet application whether heating or cooling is crucial and any interpretation of the results should account for it. For example, it was seen that a degradation of heat transfer occurs beyond the position s/W = 2, when cold air, drawn in by primary vortices from stagnant surroundings, penetrates the boundary layer. Such flow behavior manifests into a de-correlated flow and heat transfer fields.

Acknowledgement

The authors are grateful to the Petroleum Institute of Abu Dhabi for providing High Performance Computing facilities.

Reference

1. N. Zuckerman, N. Lior, Jet impingement heat transfer: physics, correlations, and numerical modeling. In: J. Hartnett, Y.I. Cho, A. Bar-Cohen (Eds.), Advances in Heat Transfer, Elsevier Inc; (2006) 565-631.
2. J.D.A. Walker, C.R. Smith, A.W. Cerra, T.L. Doligalski, The impact of a vortex ring on a wall. J. Fluid. Mech. 181 (1987) 99-140.
3. A.M. Naguib, M.M. Koochesfahani, On wall-pressure sources associated with the unsteady separation in a vortex ring/wall interaction. Phys Fluids. 16 (2004) 2613-2622.
4. M. El Hassan, H.H. Assoum, R. Martinuzzi, V. Sobolik, K. Abed-Meraim, A. Sakout, Experimental investigation of the wall shear stress in a circular impinging jet. Phys Fluids. 25 (2013) 077101.
5. D.O. Hubble, P.P. Vlachos, T.E. Diller, The role of large-scale vortical structures in transient convective heat transfer augmentation. J. Fluid. Mech. 718 (2013) 189-115.
6. E.C. Mladin, D.A. Zumbrunnen, Local convective heat transfer to submerged pulsating jets. Int J Heat Mass Transfer. 40 (1997) 3305-3321.
7. M. Tsubokura, A.T. Kobayashi, N. Taniguchi, W.P. Jones, A numerical study on the eddy structures of impinging jets excited at the inlet. Int. J. Heat Fluid Flow. 24 (2003) 500-511.
8. H.M. Hofmann, R. Kaiser, M. Kind, H. Martin, Calculations of steady and pulsating impinging jets- an assessment of 13 widely used turbulence models. Num. Heat Transf., Part B, 51 (2007) 565-583.
9. N. Uddin, S.O. Neumann, B. Weigand, Investigation of the effect of inlet velocity field excitation of turbulent impinging jet on heat transfer using large eddy simulation. In: Int. Conf. on Jets, Wakes and Separated Flows (2008) 1-8.
10. ANSYS Inc. Fluent User Guide and Fluent Theory Guide, 2011, version 14.1.
11. M. Germano, U. Piomelli, P. Moin, W.H.Cabot, A dynamic subgrid-scale eddy viscosity model. Phys Fluids. 3 (1991) 1760-1765.
12. D.K. Lilly, A proposed modification of the Germano subgrid-scale closure model. Phys Fluids. 4 (1992) 633-635.
13. T.L. Chan, C.W. Leung, K. Jambunathan, S. Ashforth-Frost, Y. Zhou, M.H. Liu, Heat transfer characteristics of a slot jet impinging on a semi-circular convex surface. Int. J. Heat Mass Transf. 45 (2002) 993-1006.

14. S. Ghosal, Mathematical and physical constrains on large-eddy simulation of turbulence. AIAA J. 37 (1999) 425-433.
15. J. Gullbrand, Grid-independent large-eddy simulation in turbulent channel flow using three-dimensional explicit filtering. In: Ann Research Briefs 2003, Center for Turbulence Research; (2003) 331-342.
16. I.B. Celik, Z.N. Cehreli, I. Yavuz, Index of resolution quality for large eddy simulations. J. Fluids Eng. 127 (2005) 949-958.
17. P. Sagaut, Large-eddy simulation for incompressible flows - An introduction. 3rd ed. Scientific Computation series, Berlin: Springer-Verlag; 2006.
18. M. Hadžiabdić, K. Hanjalić, Vortical structures and heat transfer in a round impinging jet. J. Fluid Mech. 596 (2008) 221-260.
19. Y. Addad, U. Gaitonde, D. Laurence, S. Rolfo, Optimal unstructured meshing for large eddy simulations. In: Salvetti MV, Geurts B, Meyers J, Sagaut P, editors. Quality and reliability of large-eddy simulations, ERCOFTAC Series 12(I). Springer: Netherlands (2008) 93-103.
20. Benhacine, N. Kharoua, L. Khezzar, Z. Nemouchi, Large eddy simulation of a slot jet impinging on a convex surface. Heat and Mass Transf. 48 (2012) 1-15.
21. Z, Li, L. Khezzar, N. Kharoua, Large eddy simulation of a forced turbulent jet impacting on a semi-cylinder. In: Proceedings of the ASME 2013 Fluids Engineering Summer Meeting FEDSM; (2013) V01AT03A013.
22. H.M. Hofmann, D.L. Movileanu, M. Kind, H. Martin, Influence of a pulsation on heat transfer and flow structure in submerged jets. Int. J. Heat Mass Transf. 50 (2007) 3638-3648.
23. E. Gutmark, C.M. Ho, Preferred modes and the spreading rates of jets. Phys. Fluids. 26 (1983) 2932-2938.
24. J.F. Olsen, S. Rajagopalan, R.A. Antonia, Jet column modes in both a plane jet and a passively modified plane jet subject to acoustic excitation. Exp. Fluids. 35 (2003) 278-287.
25. H. Versteeg, W. Malalasekra, An introduction to computational fluid dynamics: the finite volume method. 2nd ed. Pearson Education Limited. Edinburgh Gate. Harlow. Essx CM20 2JE; (2007).
26. M. Kornhaas, D.C. Sternel, M. Schäfer, Influence of time step size and convergence criteria on large eddy simulations with implicit time discretization. In: Salvetti MV, Geurts B, Meyers J, Sagaut P, editors. Quality and reliability of large-eddy simulations, ERCOFTAC Series 12(I). Springer: Netherlands; (2008) 119-130.
27. C. Tu, J.D. Hooper, D.H. Wood, Wall pressure and shear stress measurements for normal jet impingement. In: llth Australasian Fluid Mech. Conf. (1992) 14-18.
28. C.V. Tu, D.H. Wood, Wall pressure and shear stress measurements beneath an impinging jet. Exp Therm. Fluid Sci. 13 (1996) 364-373.
29. D.J. Phares, G.T. Smedley, R.C. Flagan, The wall shear stress produced by the normal impingement of a jet on a flat surface. J. Fluid Mech. 418 (2000) 351-375.
30. L.F.A. Azevedo, B.W. Webb, M. Queiroz, Pulsed air jet impingement heat transfer. Exp. Therm. Fluid Sci. 8 (1994) 206-213.